Combustion and Flame 160 (2013) 692–703

Contents lists available at SciVerse ScienceDirect

Combustion and Flame

journal homepage: www.elsevier.com/locate/combustflame

Heat-transfer mechanisms of lean premixed CH_4/air flame in a ceramic granular bed burner

S.I. Yang *, D.L. Hsu

Department of Power Mechanical Engineering, National Formosa University, Yunlin County 63202, Taiwan

ARTICLE INFO

Article history:
Received 28 June 2012
Received in revised form 14 November 2012
Accepted 27 November 2012
Available online 26 December 2012

Keywords:
Porous media
Premixed combustion
Instability
Firing rate
Porosity
Heat transfer mechanism

ABSTRACT

This study investigates the heat-transfer mechanism of premixed flames in a granular bed by conducting experiments and numerical simulations. The goal is to understand the heat-transfer phenomenon between the flames and the ceramic granules and among the ceramic granules themselves. This heat-transfer phenomenon involves equivalence ratios and firing rates of premixed flames because these two parameters affect the structural characteristics of flames and alter the heat transfer mechanism. These experimental results indicate that the temperature of the premixed flame increased as the firing rate increased. Additionally, the absolute propagation speed of the flame was observed to increase as the firing rate increased at a high equivalence ratio; however, the absolute propagation speed was observed to decrease as the firing rate decreased at a low equivalence ratio. At low equivalence ratios, the firing rate of the flame was relatively low and partial heat loss resulted in flame instability. The numerical simulation results indicate that changing equivalence ratios and firing rates alters the structure of the premixed flames, and the preheat characteristics of premixed flames result in the flame approaching the flameless characteristic most often seen in high-temperature air combustion. The premixed flame heat-transfer mechanism is further identified to be related to the equivalence ratio and firing rate related to the equivalence ratio and thermal radiation effects. At high equivalence ratios, thermal radiation effects have a greater influence on premixed flames. At medium equivalence ratios, preheat conductions have a greater influence on premixed flames at low firing rates; however, preheat radiation has a greater influence on premixed flames as the firing rate increases.

1. Introduction

Granular bed burners have several advantages, including low NO_x emission and high combustion efficiency [1,2]. Granular bed burner technology has been widely adopted in industrial applications such as industrial burners and fluidized bed burners. This technology enables the use of waste materials or low heating-value materials such as biomass and agricultural and forestry wastes as fuels. These materials contain a significant amount of water and numerous incombustible components, which can lead to a lower fuel heating-value and unstable combustion. Because of recent energy and environmental issues, bio-energy applications are a crucial research direction. Energy-conversion efficiency is a problem scientists must address in converting and applying biomass. To increase the energy efficiency of biomass in biomass fast pyrolysis processes, volatile matter generated in the heating process are used for combustion to provide heat and reduce the requirement for external energy. However, volatile matter generated from biomass has low heating value and contains water [3]; therefore, granular beds are used as a burner and methane and propane fuels are added to increase the stability of the flames.

Porous media combustion is based on the concept of excess-enthalpy combustion [4]: premixed flames passing through porous media transfer heat from the high-temperature zone in the downstream back to the low-temperature zone in the upstream, thereby preheating the premixed upstream mixtures. This combustion process improves the burning velocity and stability of the flames. Numerous studies have studied this process [5–15] and in these previous studies, the influence of materials and porosity on thermal conduction, convection, and radiation, the stability of flame propagation, and flammability limits during flame propagation have been studied.

Takeno and Sato [16] discovered that premixed methane–air mixtures have greater combustion efficiencies and lower lean flammability limits in porous media. Additionally, flames are stably propagated in bundle ceramic tubes and the emission is significantly lower than that of freely propagated flames. Katani et al. [17] discussed the combustion characteristics of fuels in bundled ceramic tube burners and found that the position of flames in

* Corresponding author. Fax: +886 5 631 2110.
E-mail address: IanYang@nfu.edu.tw (S.I. Yang).

0010-2180/$ - see front matter
http://dx.doi.org/10.1016/j.combustflame.2012.11.019

Nomenclature

A_p	surface of particle
C_p	specific heat capacity of mixture, kJ/kg K
D	mass diffusivity, cm^2/s
F	radiation view factor
h	convective heat transfer coefficient, kW/m^2 K
i	radiation intensity, W/m^2 sr
k	specific reaction rate constant
k_g	conduction heat transfer coefficient of gas phase, kW/m^2 K
k_s	conduction heat transfer coefficient of solid phase, kW/m^2 K
Le	Lewis number, $\lambda_g/\rho DC_{pg}$
n_p	particle number density, $1/m^3$
Nu	Nusselt number, hD/k_g
p	phase function
Pr	Prandlt number
q^v	convection heat flux, kW/m^2
q^r	radiation heat flux, kW/m^2
Re	Reynolds number
s	flame speed, m/s
T	temperature, K
x	coordinate, cm
Y	mass fraction
V	diffusion velocity, m/s
u	mixture velocity, m/s
W	molecular weight, kg/kg mole

Greek symbols

α	thermal diffusivity, cm^2/s
χ	chemical symbol for kth species
ε	porosity
ϕ	equivalence ratio
η	heat recirculation efficiency
φ	granular diameter, mm
μ	directional cosine
ν	molar concentration coefficient
ρ	density, kg/m^3
σ	Stefan–Boltzmann, kW/m^2 K^4
Γ	firing rate, kJ/s
υ	emissivity of the thermocouple
ω	reaction rate, kg mole/m^3 s

Subscript

b	backward reaction
f	forward reaction
g	gas
k	species index
r	radiation
s	solid
ab	absolute propagation flame speed
bl	black body

Superscript

‘	reactant stoichiometric coefficient
‘‘	product stoichiometric coefficient

the tube is related to both the premixed mixture flow rate and the equivalence ratio. Babkin et al. [18,19] showed identical results. They found that a premixed mixture remained stable in porous media at two different flow velocity regimes: a low-velocity regime (LVR) and a high-velocity regime (HVR). In the low-velocity regime, the propagation speed of the flames in the reaction zone and the temperature distribution were present in one ordered pattern (1 cm/s), whereas the burning velocity of gases was irrelevant to the temperature distribution in porous media in the high-velocity regime. Kim et al. [20] investigated the propagation characteristics of flames at a mild mixture velocity in porous media. The results showed that a flat flame propagated upstream through the porous media as the mixture velocity increased. Additionally, factors that affected the propagation of premixed flames in porous media included the properties of the porous materials, their porosity, and the fuel properties of the premixed mixture. These factors changed the thermal conduction, convection, and radiation properties and influenced the stability, flammability, and burning velocity of flames in the porous media. Hoffmann et al. [21] discovered that porous ceramic materials could effectively increase the flammability of fuels in a reciprocating burner. Also, the burning velocity of premixed methane–air flame in a burner that combined ceramic materials of two porosities was significantly greater than the laminar burning velocity of the adiabatic flame, and the flame appeared in the interface of the materials of different porosities.

Hanamura and Echigo [22] analyzed flame characteristics such as their stability, blow-off, flash-back, and quench in a porous media burner with spherical granules using a numerical simulation approach. Because of heat-transfer between the resultants and reactants of flames in the porous media burner, the burning velocity was increased, the lean flammability limit was expanded, and the flame stability was improved. This combustion phenomenon was extremely complex and involved reciprocal influences such as energy transfer and the chemical kinetics of the media [5]. Yoshizawa et al. [23] studied heat-transfer phenomena, including the effect of heat transfer and thermal radiation effects on flame propagation between gas and solid materials in porous media by adopting a chemical kinetics approach. Sathe et al. [9,24,25] explored the heat-transfer mechanism in fibrous porous media by adopting a chemical kinetics approach and numerical simulations. They found that different flame locations, thermal conductivity of solid materials, and thermal radiation properties influenced the stability and flame velocity of a premixed mixture. Pereira et al. [26] studied the influence of factors such as the solid-phase diffusion length scale (l_s), gas-phase diffusion length scale (l_g), and reaction length scale (l_r) on the stability and the heat-transfer properties of adiabatic premixed flame in porous media by conducting an asymptotic analysis. In their studies, they altered the equivalence ratio of the premixed mixture, as well as the convection ratio, porosity, and *Le*. Mishra et al. [27] used a two-dimensional model to investigate porous burners consisting of two overlapping materials. Mishra discovered that smaller pores could increase the volumetric heat transfer coefficient, whereas with larger pores the extinction coefficient effect was larger. Mamare et al. [28], in an investigation on burners consisting of two overlapping materials, used a one-dimensional model to calculate the temperature of the flame and found that the flame's temperature was actually lower than the adiabatic flame temperature and that the firing rate was related to its heat capacity. Mamare also used a three-dimensional model to show that the inert content in the burner greatly reduced the temperature of the flame. Heat loss during high heat generation was relatively small, leading to a comparatively high flame temperature. Sahraoui and Kaviany [29] compared their two dimensional model to one dimensional volume averaged techniques. What they concluded was that, although a two-dimensional model returned better

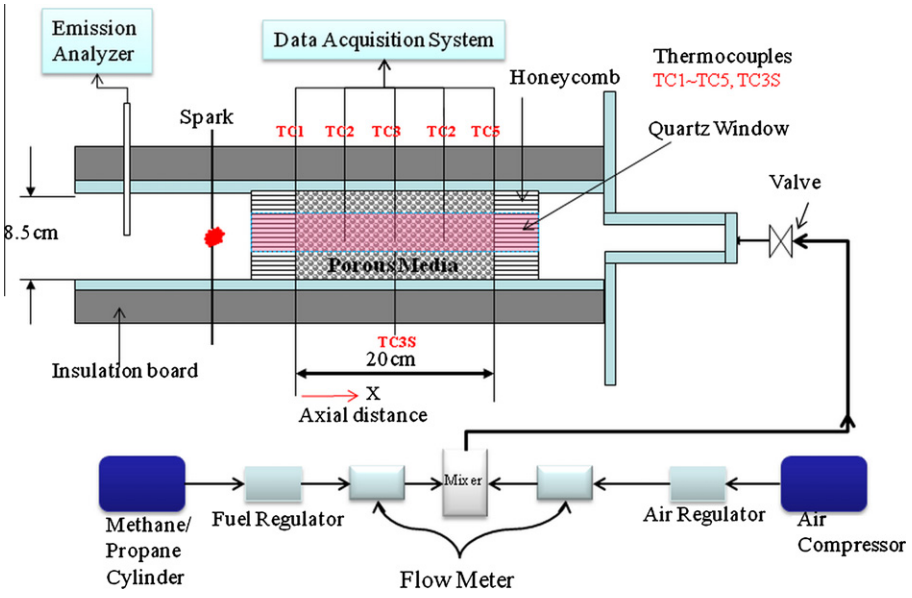

Fig. 1. Schematic of an experimental ceramic granular bed burner.

results for the calculations of the partial flame temperature and the density of the reactants, when looking at the structure of the flame, its thickness, its propagation rate, as well as the temperature gradient of solid-to-gas, a one-dimensional model yielded better results.

Most of the above studies used a single flow velocity or equivalence ratio as the properties investigated in flame propagation in a porous medium. As a result, most discovered the combustion properties of premixed flames in a porous medium, including the discovery that the flammability limit could be heightened and that the propagation could be stabilized. However, it remains unclear how the changes in both the equivalence ratio and flow velocity of premixed flames relate to the flammability limit and the stable propagation properties. The present study used experimental methods to measure the effects of the flammability limit and absolute propagation speeds of premixed flames at a wide range of mixture velocities (U) and equivalence ratios (ϕ) in ceramic granular bed burners. This study aimed to understand the structure of the flame and the properties between solid-to-gas heat transfers at different flow velocities and equivalence ratios. To accomplish this, we used numerical simulations in a single dimension to investigate the properties of the flame and the changes in the propagation mechanisms. These results will be beneficial to the future use of granular bed burners in a range of low-heat fuel applications.

2. Experimental approach

We conducted experiments using a ceramic granular burner (CGB) to investigate the propagation mechanism of lean premixed methane–air flame at different mixture velocities and equivalence ratios. We defined the location of premixed flames, investigated the unstable transfer phenomena of lean premixed methane–air flames in CGB, measured flame emissions by directly observing the color and appearance of the flames, and measured the peak temperature of lean premixed methane–air flames.

The experimental equipment used in this study can be divided into five major parts: CGB, mixture supply system, temperature acquisition system, exhaust emission analyzer, and image acquisition system (Fig. 1). The CGB was composed of a steel pipe with an internal diameter of 7.86 cm; the outer layer of the pipe was covered with heat insulation. Ceramic granules with an average diameter of 4 mm were placed inside the CGB to form a bed 20 cm long, with a ceramic honeycomb placed at each end. The physical characteristics of the CGB are listed in Table 1. A quartz glass window was placed in the middle of the steel pipes to enable the observation of flame propagation with a camera.

Table 1
Physical characteristics of the ceramic granular bed.

Specific heat	628–700 J/kg K
Diameter	4–5 mm, 25 mm
Thermal conductivity	1.44 W/m K
Contents	O_3(25.03%), SiO_2(65.97%), Fe_2O_3(0.6%)

The mixture supply system contained two sets of flow control systems that regulated the flow of fuel and air into a mixer, forming the premixed fuel and air. These premixed mixtures at a specific equivalence ratio passed through the honeycomb. The honeycombs fixed the ceramic granules at both ends of the bed and facilitated the mixing of the fuel and air. The fuel used in this study was 99.99% experimental-grade methane. The temperature acquisition system used to measure flame temperatures in the granular bed was composed of six K-type thermocouples assembled upstream of the gas at 5 cm intervals. TC3S connected the thermocouple junction and the granular pellets, and the temperature of the solid materials was measured to serve as a correction for the radiation error. The data acquisition system acquired signals transmitted from the thermocouples at a rate of 1 Hz. A Testo 350-S fuel gas analyzer with a sampling probe was positioned 3 cm downstream of the ceramic granular bed at the outlet-end honeycomb to measure the exhaust emission. Water in the exhaust emission was removed by a drying device in the analyzer.

3. Experimental results and discussion

The characteristics of the CGB are listed in Table 1. We used a premixed methane–air fuel and different volumetric flow rates to change the average premixed mixture velocity in the ceramic granules to observe the propagation of flames in the CGB. Excess-enthalpy combustion was achieved by heating the ceramic granules with heat generated from the burning premixed mixture using thermal radiation and thermal conductivity, followed by

Fig. 2. Direct photographs of CH_4/air flame front at $\phi = 0.8$ and $u = 0.41$ m/s: (a) nongranular, (b) granule size = 18 mm, and (c) granule size = 4 mm.

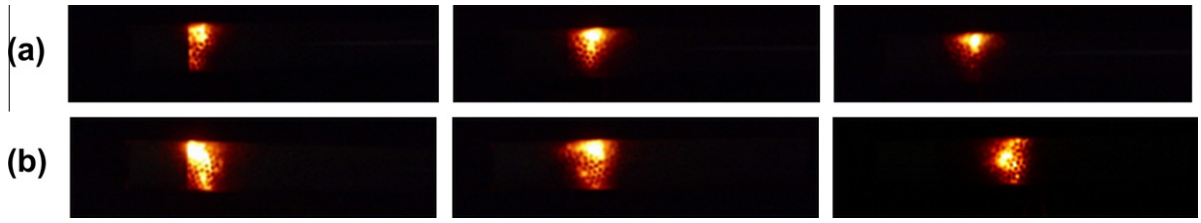

Fig. 3. Direct photographs of CH_4/air flame front with a granule size of 4 mm and $\phi = 0.6$: (a) $u = 0.31$ m/s and (b) $u = 0.51$ m/s.

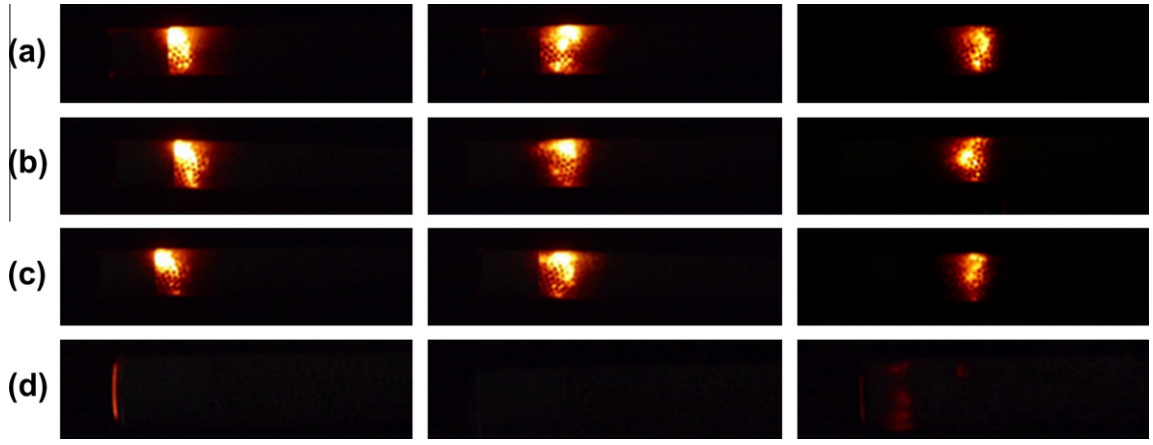

Fig. 4. Direct photographs of CH_4/air flame front at granule size of 4 mm and $u = 0.51$ m/s: (a) $\phi = 0.8$, (b) $\phi = 0.6$, (c) $\phi = 0.4$, and (d) $\phi = 0.2$.

preheating the premixed mixture using high-temperature ceramic granules.

3.1. Direct photographing

Figure 2 shows photographs of the propagation of the premixed methane–air flame at the same mixture velocity ($u = 0.41$ m/s) and at an equivalence ratio of 0.8 in the absence of ceramic granules, with large ceramic granules ($\varphi = 18$ mm), and with small ceramic granules ($\varphi = 4$ mm). The flame color varied from [1]blue to orange based on the medium of propagation. An orange flame was the result of light emitted from the ceramic granules as the flame transferred heat to the granules. Thus a more orange image signifies more heat being transferred from the flame to the granules. These results indicate that the lean premixed methane–air flame is influenced by the characteristics of the granular bed, which increase the heat loss of the flame and reduce the flame temperature. These changes subsequently reduce the flame temperature and the propagation properties of the flame. Figure 3 shows photographs of the propagation of premixed methane–air flame in 4 mm granular media with an equivalence ratio of 0.6 at different mixture velocities. As the mixture velocity increases from a low mixture velocity ($u = 0.31$ m/s) to a mild mixture velocity ($u = 0.51$ m/s), the velocity of the upstream flame propagation increases and the luminescence zone expands. Because of the presence of a stronger heat recirculation in the CGB, the enthalpy input increases as the mixture velocity increases. Therefore, the increased heat recirculation enables the flame to propagate upstream within a range of mixture velocities that allows stable propagation.

Figure 4 shows photographs of the premixed methane–air flame propagation characteristics at different equivalence ratios ($\phi = 0.8$ to 0.2) in a bed with a granule size of 4 mm and a mixture velocity of $u = 0.51$ m/s. The premixed flames at the downstream entrance (Fig. 4a and b) have similar luminescence properties: the flames are orange-red and have brilliant luminescence zones. As the flames propagate upstream, the flames in the luminescence zones appear to be discontinued and this phenomenon is more obvious as the flames progress upstream. This phenomenon is not closely related to the equivalence ratio; however, as the equivalence ratio decreases to 0.2 (Fig. 4c), the premixed flames only have a thin luminescence zone at the CGB entrance. Furthermore, the flames exhibit a broken pattern and the intensities are significantly reduced as the premixed flames propagate upstream. These results indicate that premixed methane–air flames in CGB have similar propagation characteristics downstream ($u = 0.51$ m/s and $\phi = 0.8$–0.4). As the flames propagate upstream, they are influenced by the granular bed properties and the heat-transfer characteristics of the premixed flames, resulting in local quenching. At an equivalence ratio of 0.2 (Fig. 4d), heat released by the flame under the influence of the granular bed results in a reduced luminescence zone and smaller and broken flames; additionally, the flames are more likely to be extinguished during propagation.

[1] For interpretation of color in Figs. 2 and 4, the reader is referred to the web version of this article.

3.2. Radiation error in temperature measurement

This study uses K-type thermocouples to measure the temperature of the flame. The thermocouple is struck with thermal radiation, which then causes the temperature measured by the thermocouple to deviate from the actual temperature of the flame. Thus, thermal radiation becomes an increasingly important factor to consider when measuring the absolute flame temperature in high-temperature conditions. The error caused by radiation can be estimated by considering steady-state thermodynamic equilibrium conditions for a thermocouple. If we take a 1st Law analysis of a system containing the thermocouple and ignore environmental effects on the conduction of the thermocouple, a steady-state condition yields:

$$q^v + q^r = 0 \tag{1}$$

where $q^v = hA_s(T_g - T_j)$; $q^r = \sigma\upsilon(T_s^4 - T_j^4)$.

Assuming that the surroundings may be treated as a blackbody, the first law for a system consisting of the thermocouple is

$$hA_s(T_g - T_j) = FA_s\sigma\upsilon(T_j^4 - T_s^4) \tag{2}$$

$$T_g = T_j + \frac{F\sigma\upsilon}{h}(T_j^4 - T_s^4) \tag{3}$$

where υ is the emissivity of the thermocouple, and h is the convection coefficient. These values change as T_g changes. Thus, they can be obtained through a numerical iteration algorithm. To test for effects caused by radiation error in the thermocouples used in this study, we set two thermocouples, TC3 and TC3S, in the center of the CGB (see Fig. 1). TC3 was set in the center of the CGB in such a way as to avoid contact with the ceramic granules, while the junction TC3S was set in contact with the ceramic granules and adhered to the solid material with fire resistant glue. TC3 and TC3S were both set in the center of the burner without contacting the burner. The temperatures measured are represented by T_j and T_s. T_g is the temperature value obtained from Eq. (3). Figure 5 shows the time–temperature relationship of data obtained from the test on premixed methane–air with $\phi = 0.9$ and $u = 0.57$ m/s. When the flame is situated upstream, the difference in the T_j and T_s values is small. However, when the flame propagates upstream, the difference between the two values increases, and when the flame propagates upstream through the thermocouple, the temperature decreases. This is largely due to the large heat capacity of the ceramic granules. When the flame passes through the thermocouple, the radiation error between the measured temperature and the actual flame temperature is less than 3%. The presence of this difference does not affect the observed position of the flame propagation, though it does influence the measured temperature of the flame. To account for this derivation in the measured and actual temperatures, this study uses the temperature after the correction for radiation error has been applied as the actual flame temperature.

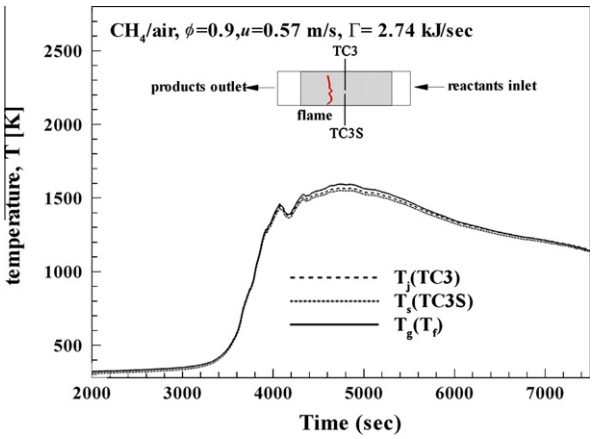

Fig. 5. Temperature profiles of thermocouple junction, solid and gas.

3.3. Temperature trace of flame propagation

To further measure the propagation characteristics of premixed flames in CGB, the firing rate (Γ, kJ/s) of a premixed flame in a CGB is defined as follows: firing rate = High heating value, HHV of methane x mole fraction of the mixture. Under the operation conditions of the premixed mixture at $\phi = 0.9$, $u = 0.26$ m/s, and a firing rate of 1.24 kJ/s, the rate of heat loss in a premixed flame is high as it contacts the ceramic granules because of the low mixture velocity and firing rate. Consequently, the flame can only propagate to the entrance of the granular bed and cannot propagate further upstream (Fig. 6a); the maximum flame temperature is approximately 980 K. Under the operating conditions of a premixed mixture at $\phi = 0.9$ and by increasing the mixture velocity to 0.57 m/s and the firing rate to 2.74 kJ/s, the premixed flame propagates from the downstream end toward the upstream end and enters the CGB. The flame propagates very slowly and widely in the CGB; the maximum flame temperature is 1610 K and the time the flame propagates from TC1 to TC5 is 772 s (Fig. 6b). The heat-transfer characteristics of the flame in the granular bed determine whether the flame can be propagated through the granular bed and also influences the properties of flame propagation, such as the propagation time, temperature, and emission.

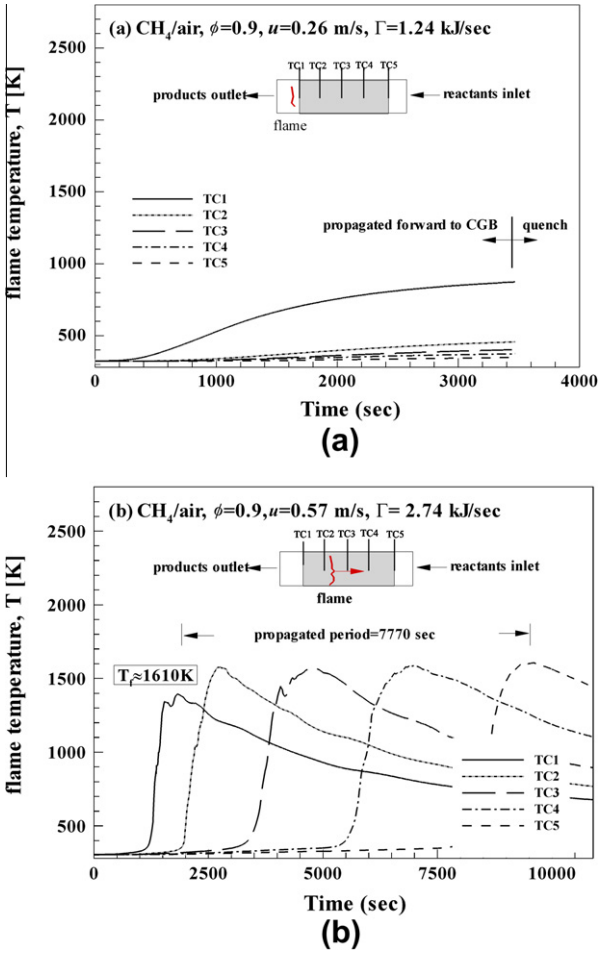

Fig. 6. Temperature trace of premixed flames propagated in a CGB: (a) quenching and (b) propagation.

3.4. The effect of mixture velocity and firing rate on operating condition limits

Figure 7a and b shows the operating boundary of the premixed methane–air mixture in the CGB. The error bars in the figures represent the root-mean square values from five mixture-velocity experiments. Figure 7a shows the effects of the mixture velocity on the flame propagation properties. The maximum equivalence ratio of the premixed methane–air in the CGB is 0.9 and the minimum flammability limit is 0.5. Under the operating conditions of a high equivalence ratio ($\phi = 0.9$), the mixture velocity of the premixed methane–air ranges from 0.23 to 1.15 m/s. At $\phi = 0.5$, the operating range of the mixture velocity is from 0.49 m/s to an average maximum velocity of 0.78 m/s; the average operating range of the mixture velocity is reduced significantly. This result indicates that as the equivalence ratio decreases, the unit volume of fuel decreases; that is, the enthalpy decreases. Therefore, as the premixed flame propagates in the CGB, heat generated from burning and from heat transferred among the ceramic granules influence the CGB operating range.

At a low mixture velocity, the firing-rate operating range of the premixed mixture is approximately 1.30 kJ/s (Fig. 7b), indicating that the firing rate of the premixed mixture must be greater than the threshold value for the premixed flame to propagate in the CGB at a low mixture velocity. Additionally, the operable firing-rate range increases as the equivalence ratio increases at a high mixture-velocity operating range. At a low mixture velocity and low firing-rate limit, a premixed flame would cease propagation and blow off in the CGB due to the influence of heat loss. As the mixture velocity and firing rate increase, preheated fuel is propagated stably in the CGB because of the heat-transfer characteristics of the premixed flame and the CGB; the flame is a submerged flame. However, as the mixture velocity and firing rate increase, the mixture velocity exceeds the propagation velocity of the premixed flame in the CGB; consequently, the premixed flame is unable to propagate upstream and results in flame blow-out. The described phenomena are related to the heat-transfer characteristics between the premixed flames and the CGB.

3.5. Flame temperature in a ceramic granular burner

Figure 8a displays the relationship between different mixture velocities and the flame temperature (T) in the CGB at different equivalence ratios. The T of the premixed methane–air at $\phi = 0.9$ and $u = 0.881$ m/s is 1830 K, and T decreases as the mixture velocity decreases. At $u = 0.248$ m/s, T is 1122 K; at $\phi = 0.5$ and $u = 0.495$ m/s, T is 1119 K; as u increases to 0.877 m/s, T reaches 1361 K. As u or ϕ changes, the firing rate changes correspondingly; therefore, T also changes. The results indicate that at equivalence ratios between 0.5 and 0.9, the minimum T at which the flame can be propagated in the CGB is approximately 1100 K; flames with temperatures lower than this value cannot propagate and are extinguished. Figure 8b shows the relationship of the

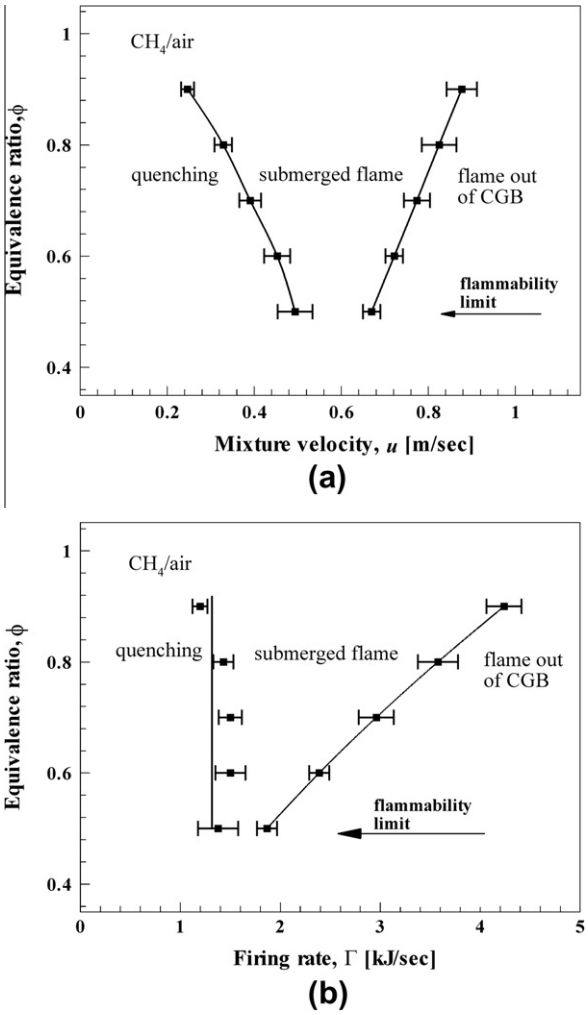

Fig. 7. CGB operating boundary equivalence ratio versus (a) mixture velocity, u [cm/s] and (b) firing rate, Γ [kJ/s].

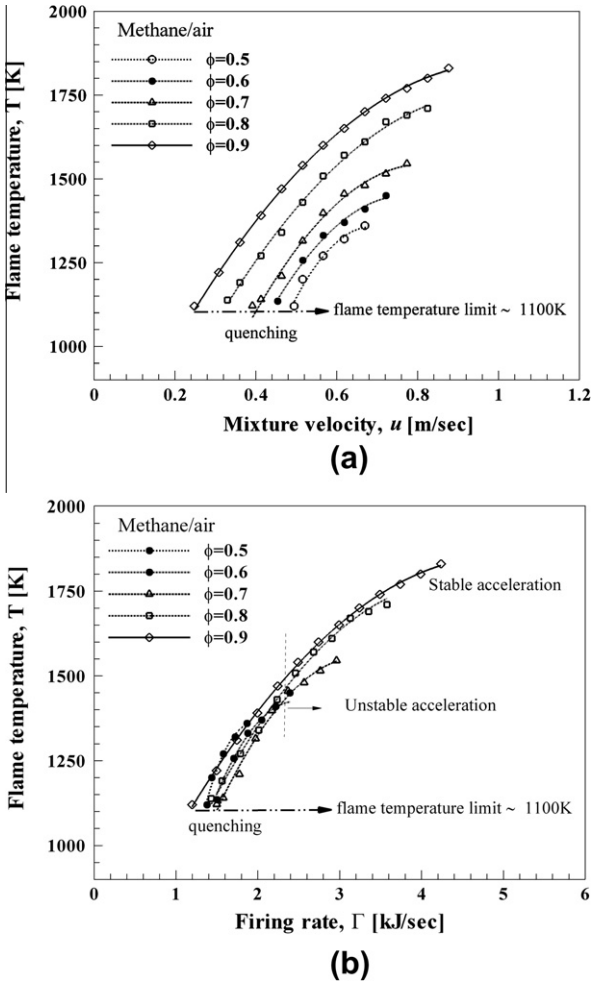

Fig. 8. Flame temperature of submerged flames in the ceramic granular bed burner with (a) mixture velocity, u [cm/s] and (b) firing rate, Γ [kJ/s].

temperature of premixed mixture flames and firing rates at different equivalence ratios. The minimum temperature of flame propagation is 1100 K and the minimum firing rate is between 1.17 and 1.49 kJ/s at low firing rates (<2.34 kJ/s). As the firing rate increases, the T increases in a linear pattern, but as the firing rate exceeds 2.34 kJ/s and in low equivalence ratios ($\phi < 0.7$), the temperature curve of the premixed flames displays an increased bending pattern as the firing rate increases. Based on the data shown in Figs. 3 and 4, the decrease in flame temperature is inferred to be caused by the decrease of firing rate and heat loss.

3.6. Absolute propagation speed

Based on the discussed experimental results, a relationship between the propagation time and the firing rate as flames propagate in the CGB was found by directly observing the propagation of premixed flames in the CGB and measuring the flame temperature. Therefore, the time difference between TC1 and TC5 was used as a reference to calculate the absolute propagation speed of flames in the CGB. Figure 9 shows the relationship between the firing rate of premixed methane–air flame in the CGB and the absolute propagation speed of the flame at different equivalence ratios. At high equivalence ratios ($\phi = 0.9$), the absolute propagation speed of the premixed flame increases from 0.0008 cm/s to a maximum of 0.0051 cm/s as the firing rate increases; the greater the firing rate, the higher the increase of the absolute propagation speed. At an equivalence ratio of 0.8, the absolute propagation speed of the premixed flame is 0.0007 cm/s, with a maximum speed of 0.0027 cm/s. Although the propagation speed increases as the firing rate increases, the rate of increase is reduced in comparison to the rate of increase when the equivalence ratio is at 0.9. However, as the relationship between the equivalence ratio decreases to 0.7, the absolute propagation speed of the premixed flame and firing rates become insignificant; the absolute propagation speed is between 0.00057 and 0.0006 cm/s. As the equivalence ratio decreases to 0.5 and 0.4, the absolute propagation speed of the premixed flame decreases from 0.00058 cm/s to 0.00051 and 0.0004 cm/s, respectively. Factors that influence the absolute propagation speed of premixed flames in the CGB are complex and include the granule characteristics and the fuel characteristics of the premixed flames. These characteristics have influences on thermal radiation, thermal convection, and the reaction zone of the premixed flame in the CGB. Numerous previous studies have discussed the radiation and convection properties of porous media burners. In this study, by using different equivalence ratios and flow rates for fuels and different firing rates of premixed flames, we observed that different equivalence ratios of premixed flames result in different absolute propagation speeds. The free flame of the lean premixed methane–air has a *Le* that is less than one and unstable propagation properties. However, because the propagation of lean premixed flame in the CGB is influenced by the ceramic granules, a preheating property of the flame is induced. This property changes the thermal diffusivity and mass diffusivity of the premixed flames. As a result, the *Le* for the premixed flames at higher equivalence ratios (0.9 and 0.8) changes from less than one in free flame to greater than one. Additionally, high firing rates induce greater thermal radiation and preheat the ceramic granules, thereby accelerating the propagation of the premixed flame. Conversely, at low equivalence ratios (0.4 and 05), premixed flames have lower flame temperatures and lower firing rates. As a result, the preheating effect is insignificant and the *Le* of the premixed flame in the CGB is still less than one. Additionally, the propagation of premixed flames is unstable or the flames can be extinguished at lower firing rates. These results indicate that at high equivalence ratios (0.9 and 0.8), the high firing rate of the premixed methane–air flames effectively preheats the CGB. Consequently, the *Le* of the flame is changed and the stability and the propagation speed of the flame increases. However, at low equivalence ratios, the firing rate is lower and cannot effectively preheat the ceramic granular bed. Consequently, the flame instability increases, heat loss on the flame is increased, and the absolute propagation speed is reduced or even stopped. These studies thus provide an understanding of the burning mechanism of flames in porous media.

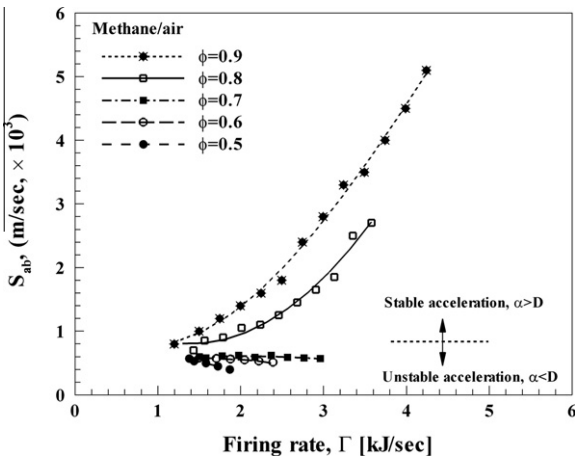

Fig. 9. The absolute velocity of premixed methane/air flame propagated in a ceramic granular bed burner with firing rate.

3.7. Emission of premixed flame in ceramic granular burner

Figure 10 shows the relationship between the premixed flame emission and firing rate. The exhaust emission of the premixed flame is corrected to a 6% O_2 concentration. Figure 10a displays the relationship between NO_x and firing rate. As shown in the figure, because NO_x emitted from the premixed flame is at a low firing rate (<2.18 kJ/s) and the premixed flame temperature is less than 1400 K, NO_x emission is less than 5 ppm and does not change as the equivalence ratio changes. However, as the firing rate exceeds 2.18 kJ/s and the premixed flame temperature exceeds 1400 K, the amount of NO_x emitted from the premixed flame increases as the firing rate increases. The generated NO_x is primarily thermal NO_x.

The NO_x emissions produced during our experiments are primarily the product of two nitrogen oxides forming nitric oxide (NO) and nitric dioxide (NO_2). Most of the NO_2 is a product of the flame zone, and a large part of that is further converted to NO in the postflame zone. This is why most NO_2 is seen as a temporary product of the flame. In many industrial applications, large volumes of cold air are mixed with the high-temperature products of combustion for the quenching of the NO_2. This causes large amounts of NO_2 to be produced downstream of the flame. The present study does not use large volumes of cold air to dilute the products of combustion at the CGB opening, and thus the NO_x measured by this study is mostly in the form of NO, specifically prompt NO and thermal NO. Prompt NO primarily forms at the flame front, while there is a significant relationship between the formation of thermal NO and flame temperature. As the Zeldovich mechanism has shown, thermal NO forms when oxygen-containing air exceeds 1300 °C. In our own study, when the firing rate was <2.18 kJ/s and the premixed flame temperature was lower than 1400 K, the flame was relatively diffuse, the flame temperature was low, and there was a possibility of partial extinguishing of the flame. Within this range of operation, CO concentration was rather high, and NO_x concentration was rather low, with most of the NO_x coming in the form of prompt NO. When the firing rate was >2.18 kJ/s and the premixed flame temperature was higher than 1400 K, the flame zone was concentrated and there was very little extinguishing of the flame. Because of this, CO concentration was low, and prompt

NO concentration increased with the size of the area of the flame. When the temperature was steadily increased, the concentration of thermal NO also steadily increased to the extent that it became the primary source of NO_x.

The heat-transfer phenomenon between the flame and the granules affects the measurement accuracy of the flame temperature in addition to affecting the propagation of the flame itself. In general, the combustion temperature measured from the thermocouple on the reactor is used, though its measured value is altered from the actual value by environmental radiation. Because of this, non-intrusive gas measurement methods [30,31] should be developed to mitigate the errors produced at the probes, such as those stemming from conduction and radiation. In summary, the firing rate can change the shape, temperature, operating boundary, absolute propagation speed, and emission of premixed flames in CGB. Changes in these propagation properties are primarily caused by heat transfer between the premixed flames and the granular bed induced by firing rates. Changes in these propagation properties further influence the structure of premixed flame and alter the mechanism of flame propagation. Therefore, another focus of this study was to conduct numerical simulations on ceramic granular beds to investigate the structural changes of premixed flame under the influence of thermal radiation and conduction.

4. Numerical approach

To advance the understanding of the burning mechanism of premixed flame in a CGB, PREMIX software [34] and GRI 1.2 were employed to compute the one-dimensional flame structure of premixed methane–air flame in the CGB. The geometric shape of the flame structure in the CGB with premixed methane–air of various velocities at an initial temperature of 300 K was calculated. We made the following assumptions to simplify the calculation process [29,32,33]:

a. Steady isobaric, quasi-one-dimensional flame propagation.
b. Gas radiation is neglected.
c. The solid radiates are not considered.
d. Catalytic effects are not considered.
e. Dufour and Soret effects are neglected.
f. Buoyancy effects are neglected.
g. The permeability of the porous matrix is so large that the pressure drops because the interaction with the matrix is negligible.
h. Compressibility effects are neglected.

The governing equation contains thermal conduction, convection, radiation, and combustion. Additionally, gas-to-solid and solid-to-solid conductions are considered. Therefore, the energy equations for these two conductions are formulated as described in the following sections.

4.1. Governing equations

Continuity:

$$\frac{d}{dx}(\rho u\varepsilon) = 0 \tag{4}$$

where ρ is the density of fuel mixture, u is the average velocity of fuels in the granular bed, and ε is the porosity.

Species conservation:

$$\rho u\varepsilon\frac{dY_k}{dx} + \frac{d}{dx}(\rho\varepsilon Y_k V_k) = \varepsilon\dot{\omega}W_k \quad (k = 1,2,3,\ldots,K) \tag{5}$$

where $\dot{\omega}_k$ is the production rate of the kth component. The general formula for the ith formation reaction can be presented as follows:

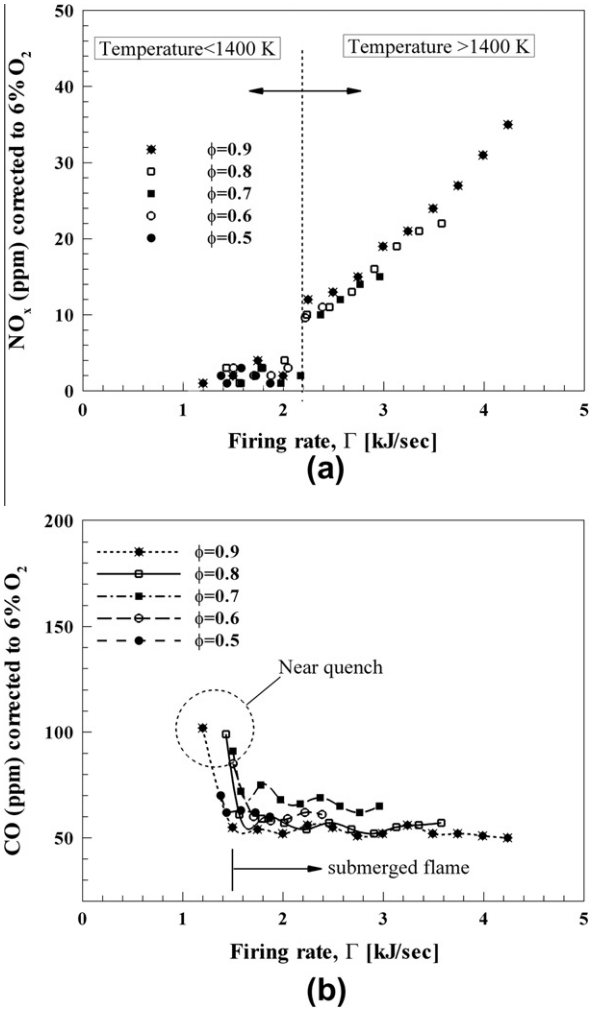

Fig. 10. Emission corrected to 6% O_2 of the premix flame in a ceramic granular bed burner: (a) NO_x and (b) CO.

$$\sum_{k=1}^{k} v'_{ki}\chi_k \leftrightarrow \sum_{k=1}^{k} v''_{ki}\chi_k \quad (i = 1,2,3,\ldots,I) \tag{6}$$

The net production rate of the kth component $\dot{\omega}_k$ is presented as follows:

$$\dot{\omega}_k = \sum_{i=1}^{I}(v''_{ki} - v'_{ki})\left(k_{fi}\prod_{k=1}^{k}[\chi_k]^{v'_{ki}} - k_{ri}\prod_{k=1}^{k}[\chi_k]^{v''_{ki}}\right) \tag{7}$$

where k_{fi} can be presented as follows:

$$k_{fi} = A_i T^{\beta_i}\exp\left(-\frac{E_i}{R_u T}\right). \tag{8}$$

where k_{fi} and k_{ri} are the constants of forward and back reactions in the ith chemical reaction, respectively.

Energy equations include a gas-phase equation and a solid-phase equation:

Gas phase

$$\rho u\varepsilon C_p\frac{dT_s}{dx} + n_p A_p h(T_g - T_s) + \varepsilon\sum_{k=1}^{k}\rho Y_k V_k C_{pk}\frac{dT_g}{dx} = -\varepsilon\sum_{k=1}^{k}\dot{\omega}h_k W_k + \frac{d}{dx}\left(\varepsilon k_g\frac{dT_g}{dx}\right) \tag{9}$$

where A_p is the surface area of a spherical particle and n_p is the particle density ($1/m^3$).

Solid phase

$$(1-\varepsilon)\frac{d}{dx}\left(k_s\frac{dT_s}{dx}\right)+n_pA_p(T_g-T_s)=\frac{dq^r}{dx} \tag{10}$$

where q^r is thermal radiation flux.

Thermal radiation equation:

$$\mu\frac{\partial i(x,\mu)}{\partial x}+(\sigma_g+\sigma_s)i(x,\mu)=\sigma_g i_b(T_s)+\frac{\sigma_s}{2}\int_{-1}^{1}p(\mu,\mu')i(x,\mu)d\mu' \tag{11}$$

The thermal radiation flux q^r in the solid-phase energy equation is presented as follows:

$$q^r=2\pi\int_{-1}^{1}i(x,\mu)\mu' d\mu' \tag{12}$$

4.2. Boundary conditions

Based on the experimental conditions of this study, the boundary conditions for the numerical simulation are defined below. The assumption is made that the temperature at the entrance and the concentration of substances are known. Therefore

Inlet

$$Y_k=Y_{ki},\quad T_g=T_i\quad \text{at } x=x_i \tag{13}$$

The exit temperature and the concentration of substances have insignificant changes:

Outlet

$$\frac{dY_k}{dx}=\frac{dT_g}{dx}=0\quad \text{at } x=x_e \tag{14}$$

We take the heat transfer, thermal convection, and thermal radiation effects among solid particles in ceramic granular bed into consideration. The thermochemical and transfer properties among gases can be obtained from Chemikin [34] and Tranfit [35] and can be calculated by the C-1 chemical kinetics mechanism [35]. The solid-to-solid radiation heat transfer is calculated by using an optically thick approximation [36]. Radiation properties, such as albedo, emissivity, and extinction coefficient are assumed to be unity. Additionally, the heat-transfer coefficient for forced convection [37] of the granular bed is considered and can be calculated using the following equation:

$$Nu=2.19(\mathrm{RePr})^{1/3} \tag{15}$$

5. Numerical simulation results and discussions

The relationship between the firing rate and the propagation mechanism of the premixed flame generated by different equivalence ratios and the premixed methane–air flame at different mixture velocities are described in the following sections.

5.1. The structure of a premixed flame in a ceramic granular burner

The propagation properties of premixed flames in a CGB are influenced by firing rates and result in changes in flame temperature, absolute propagation speed, and emission. Therefore, we adopt the numerical simulation method to discuss the effect of different equivalence ratios and mixture velocities on flame structure. Figure 11a and b shows the propagation of the premixed methane–air flame at an equivalence ratio of 0.9, $u = 0.52$ m/s, and a high firing rate of 2.49 kJ/s. The temperature distribution of the fuels slowly starts increasing from a position 14 cm upstream to 9.1 cm, after which the distribution rapidly increases downstream. The temperature increases rapidly near the reaction zone and the

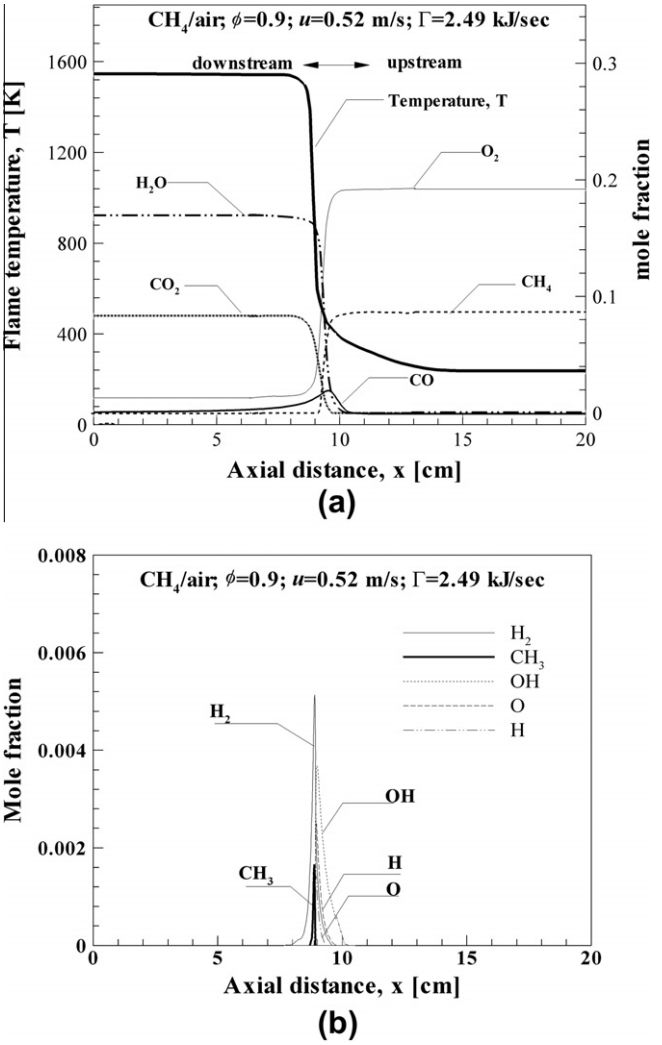

Fig. 11. High firing rate flame structure of premixed methane/air flame, $\phi = 0.9$, $u = 0.52$ m/s, firing rate = 2.49 kJ/s: (a) major species mole fraction and (b) minor species mole fraction.

amount of CH_4 and O_2 similarly increases. The peak value of CO appears in the middle section of the CGB but slightly downstream (Fig. 11a). As shown in Fig. 11b, the peak H_2 value is the highest among all minor species, appearing at 8.91 cm. CH_3 is an indicator of the reaction zone; its peak value is at 8.85 cm and it has an extremely narrow distribution. At a mixture velocity of 0.52 m/s, an equivalence ratio of 0.7, and a firing rate of 1.97 kJ/s (Fig. 12a), the flame temperature starts increasing slowly from 19 cm upstream to 10.7 cm, after which, the temperature increases rapidly to 1328 K. The amount of H_2O begins to increase at 10.89 cm but CO_2 does not appear until 0.28 cm. The peak value of CO appears at 10.05 cm, the peak value of H_2 appears at 9.37 cm, and the peak value of CH_3 appears at 9.68 cm (Fig. 12b). Because the equivalence ratio is 0.7, the mixture velocity decreases to 0.41 m/s, the firing rate decreases to 1.57 kJ/s, and the flame temperature distribution is wider; the flame structure is shown in Fig. 13a and b. The flame temperature starts increasing at 20 cm and the highest temperature appears near 8.13 cm. The concentrations of CH_4 and O_2 start decreasing at 13.7 cm, the concentrations of H_2O and CO_2 start increasing at 12.7 and 11.9 cm, respectively, and the peak value of CO appears at 11.73 cm. As shown in Fig. 13b, the distributions of minor species of the flame are wider and propagate upstream; the peak values also tend to appear upstream.

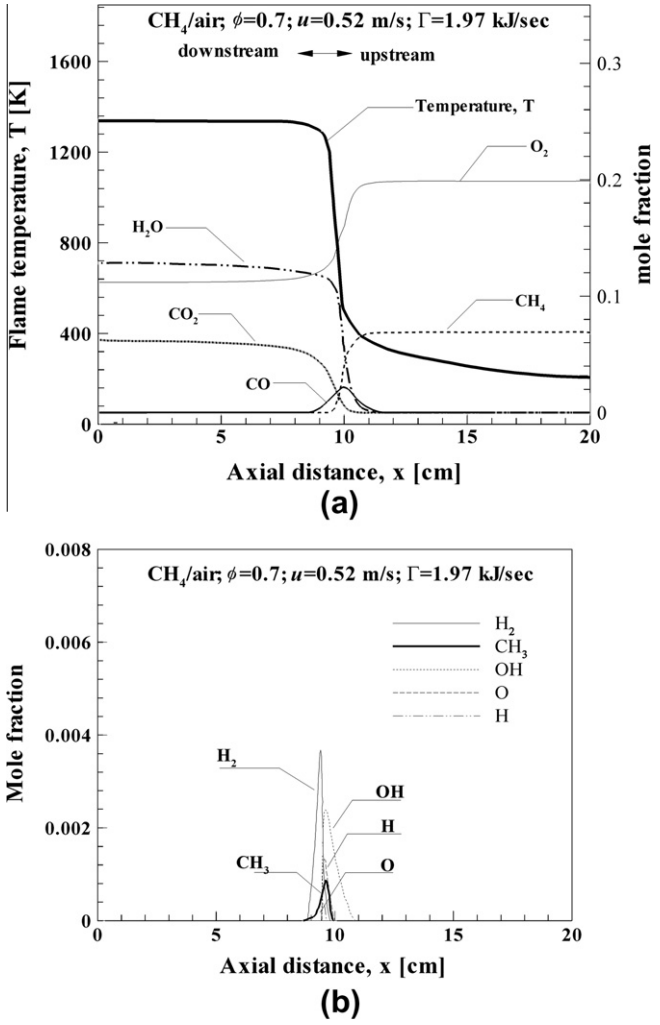

Fig. 12. Moderate firing rate of a flame structure of premixed methane/air flame, ϕ = 0.7, u = 0.52 m/s, firing rate = 1.97 kJ/s: (a) major species mole fraction and (b) minor species mole fraction.

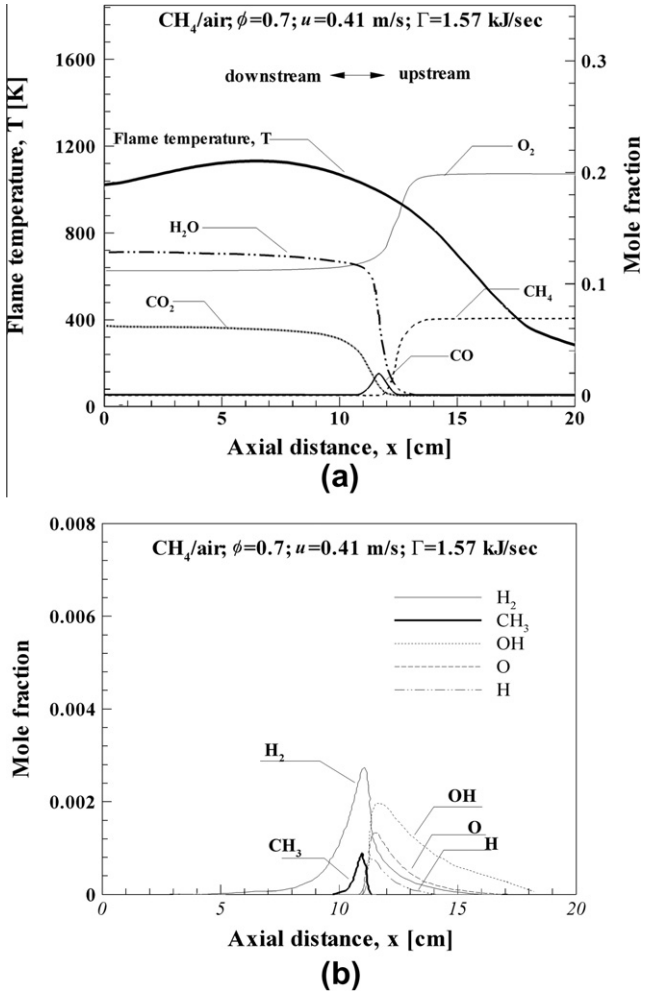

Fig. 13. Low firing rate of a flame structure of premixed methane/air flame, ϕ = 0.7, u = 0.41 m/s, firing rate = 1.57 kJ/s: (a) major species mole fraction and (b) minor species mole fraction.

The peak CO and CH_3 values in the reaction zone of the three types of premixed flames are compared. As the firing rate decreases and the flames propagate upstream, the peak values decrease and the peaks become broader. These phenomena indicate that the reaction zone of premixed methane–air flames become wider as the firing rate is reduced by the preheating effect of the ceramic granules. Its reaction zone is not obvious and reflects the flameless phenomenon of high-temperature air combustion. Therefore, the thermal radiation generated by the flame is also greater and results in an unstable flame. However, the partial heat loss in the preheated premixed mixture increases the flammability of the flame. These results are consistent with those in the study conducted by Kim et al. [20].

5.2. Heat-transfer mechanism of lean premixed flames in a ceramic granular burner

To enhance the understanding of the heat-transfer mechanism of premixed flames in a CGB, we investigated the heat-transfer properties of premixed flames in a granular bed with three dimensionless parameters [38]: (1) heat-recirculation efficiency, η; (2) preheat-conduction efficiency, ψ_c; and (3) preheat-radiant efficiency, ψ_r. Heat-recirculation efficiency is defined as the ratio between heat transferred to the gas in the preheat zone and the firing rate:

Heat recirculation efficiency,

$$\eta = \frac{\text{solid-to-gas convection in preheat zone}}{\text{firing rate}} \tag{16}$$

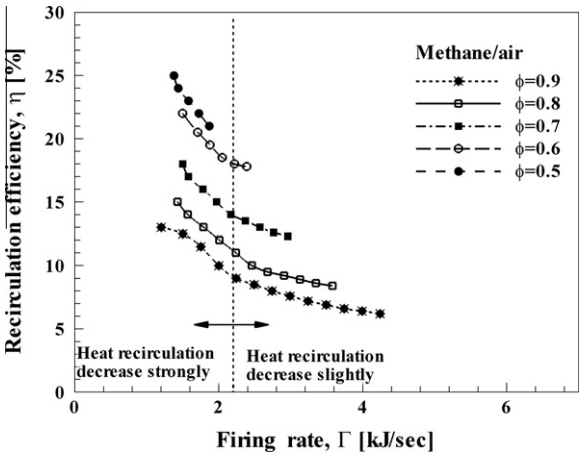

Fig. 14. Heat recirculation efficiency as a function of flame speed ratio for a range of equivalence ratios.

Solid ceramic granules transfer heat to the premixed mixture and to the ceramic granules to heat the flame in the preheat zone. The preheat-conduction efficiency and the preheat-radiant efficiency are defined as follows:

Preheat conduction efficiency,

$$\Psi_c = \frac{\text{solid conduction into preheat zone}}{\text{firing rate}} \tag{17}$$

Preheat radiant efficiency,

$$\Psi_r = \frac{\text{radiation into preheat zone}}{\text{firing rate}} \tag{18}$$

The parameters described above are used to investigate the heat transfer properties of flames in a CGB at different operating conditions to advance the understanding of the heat-transfer mechanism of premixed flames.

Figure 14 shows the relationship between the firing rate of the premixed mixture in a CGB and the heat-recirculation efficiency. Premixed mixtures have greater heat-recirculation efficiencies at low equivalence ratios and at operable firing rate ranges from 1.38 to 1.87 kJ/s. However, the heat-recirculation efficiency decreases as the equivalence ratio increases and as the operable range increases from 1.20 to 4.24 kJ/s. In low firing-rate operating limits, the firing-rate operating conditions at different equivalence ratios are between 1.20 and 1.52 kJ/s and the heat-recirculation efficiency increases as the equivalence ratio decreases. At a high firing-rate operating limits and high equivalence ratio (ϕ = 0.9), the high firing rate is 4.24 kJ/s and the heat-recirculation efficiency increases from 6.2% to 25.1% as the equivalence ratio decreases (ϕ = 0.5). At firing rates lower than 2.2 kJ/s, heat-recirculation efficiency decreases rapidly as the firing rate increases, but as the firing rates exceed 2.2 kJ/s, the amount by which the heat-recirculation efficiency decreases is reduced. These results are consistent with the data shown in Figs. 7 and 8, indicating that as the firing rate exceeds 2.2 kJ/s, the decrease of heat recirculation efficiency is reduced. This phenomenon indicates that the amount of heat energy a flame can provide for a CGB decreases and may be caused by local quenching of the flame, resulting in an increase of unstable flame propagation.

We further analyzed the influence of different heat-transfer properties on flame propagation mechanisms. Figure 15 shows the relationships between firing rate and heat-recirculation efficiency, preheat-conduction efficiency, and preheat-radiant efficiency at different equivalence ratios. Figure 14a shows these relationships at an equivalence ratio of 0.9. The heat recirculation efficiency of premixed methane–air at ϕ = 0.9 decreases as the firing rate increases. Similarly, the preheat-conduction efficiency decreases as the firing rate increases. However, preheat-radiant efficiency does not change as the firing rate increases. The value of the preheat-radiant efficiency is approximately 5.74% and is greater than the preheat-conduction efficiency. Because of the greater firing rate at an equivalence ratio of 0.9, the heat-recirculation efficiency of premixed flame is lower than that in the CGB. However, preheat-conduction efficiency decreases and is lower than the preheat-radiant efficiency as the firing rate increases. Therefore, the preheat-radiant efficiency dominates the heat recirculation in premixed flames at high equivalence ratios.

As the equivalence ratio decreases to 0.7 and when the firing rate of the premixed flame is less than 2.2 kJ/s, the preheat-conduction efficiency rapidly decreases as firing rate increases, although the preheat-conduction efficiency is greater than the preheat-radiant efficiency (Fig. 15b). As the firing rate exceeds 2.2 kJ/s, preheat conduction gradually decreases, falling below the preheat-radiant efficiency. Therefore, at a medium equivalence ratio (ϕ = 0.7) and low firing rates, preheat-conduction efficiency dominates the heat-recirculation efficiency in a premixed flame. However, as the firing rate increases, preheat-radiant efficiency becomes more dominant (Fig. 15b).

As shown in Fig. 15c, preheat-conduction efficiency decreases as the firing rate increases at a low equivalence ratio (ϕ = 0.5). The preheat-conduction efficiency is greater than the preheat-radiant efficiency, and the preheat-recirculation efficiency of premixed methane–air is dominated by conduction. These results

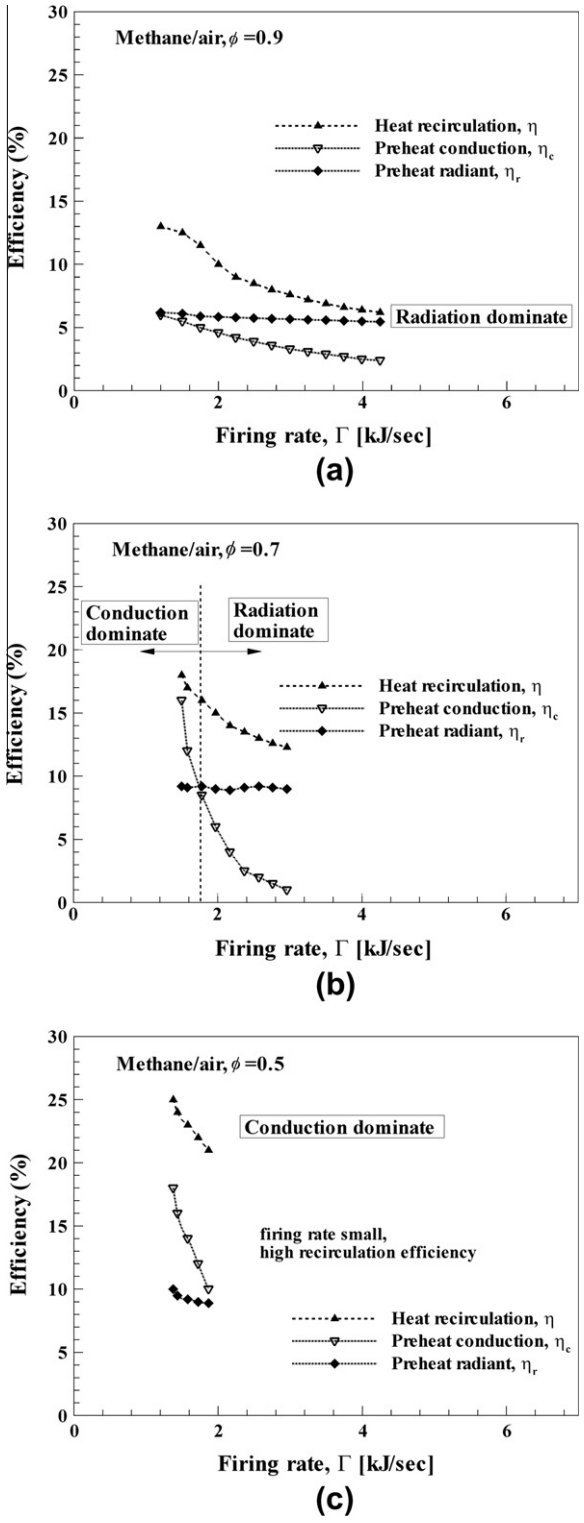

Fig. 15. Difference mechanisms of heat recirculation of premixed methane/air: (a) ϕ = 0.9, (b) ϕ = 0.7, and (c) ϕ = 0.5.

are consistent with the findings of Sathe et al. [9] and Barra and Ellzey [40].

6. Conclusions

This study investigated the propagation mechanism of premixed methane–air flame in a CGB by conducting experiments and numerical simulations. Under the influence of ceramic granules, premixed flames transfer heat between flames and ceramic granules and among ceramic granules. This heat-transfer phenomenon is function of the equivalence ratio and firing rate of premixed flames, because these two parameters affect the structural characteristics of the flames and result in alterations in the heat-transferring mechanisms. The experimental and numerical results revealed the following:

1. The experimental results indicate that ceramic granules change the heat-transfer characteristics of premixed flames, as well as their shape and color. Additionally, the equivalence ratio and mixture velocity can also affect the appearance of flames.
2. The temperature of the premixed flame increased with the increase of firing rate. Additionally, the absolute propagation speed of the flame was observed to increase as the firing rate increased at a high equivalence ratio. However, the absolute propagation speed was observed to decrease as the firing rate decreased at a low equivalence ratio. These phenomena were induced by two factors. At low equivalence ratios, the firing rate of a flame was relatively low and partial heat loss resulted in flame instability. However, the characteristics of the preheat flame changed at high equivalence ratios when the flame temperature was greater than 1400 K.
3. The change of the preheat flame characteristics altered the mass diffusivity and thermal diffusivity, and the *Le* in free flames increased from less than one to greater than one, escalating the flame propagation instability. Conversely, the preheat characteristics of flames at low equivalence ratios were insignificant; therefore, *Le* was still less than one. Also, the heat loss of the flame resulted in unstable flame propagation.
4. The numerical simulation results indicate that changing equivalence ratios and firing rates alter the structure of a premixed flame, and the preheat characteristics of the premixed flame causes the flame to approach a flameless characteristic of high-temperature air combustion (HiTAC). The heat-transfer mechanism of a premixed flame is further identified to be related to its equivalence ratio and firing rate.
5. At high equivalence ratios, thermal radiation effects have a greater influence on premixed flames. At medium equivalence ratios, preheat conductions have a greater influence on premixed flames at low firing rates, but as the firing rate increases, preheat-radiant efficiency has greater influence. At an equivalence ratio of 0.5, the premixed flame is primarily affected by preheat conduction, which results in various heat propagation characteristics.

In summary, premixed flames are affected by ceramic granular bed burners, in that ceramic granular bed burners can expand the flammability limits of a premixed mixture, reduce emissions, and increase firing rate; ceramic granular bed burners can therefore be applied to low heating-value fuels.

Acknowledgments

The authors would like to thank the National Science Council, Taiwan, for financially supporting this research under NSC 101-3113-E-008-004 and NSC 100-2221-E-150-085. Mr. E.W. Yang and Z.W. Zhang are appreciated for their experimental assistance.

References

[1] M. Pilawska, C.J. Butler, A.N. Hayhurst, D.R. Chadeesingh, Combust. Flame 127 (2001) 2181–2193.
[2] W. Wu, A.P. Dellenback, P.K. Agarwal, H.W. Haynes Jr., Combust. Flame 140 (2005) 204–221.
[3] S.I. Yang, C.Y. Wu, K.H. Chen, Adv. Mater. Res. 328–330 (2011) 881–886.
[4] F.J. Weinberg, Nature 233 (1972) 239–241.
[5] J.R. Howell, M.J. Hall, J.L. Ellzey, Prog. Energy Combust. Sci. 22 (1996) 121–145.
[6] R. Mital, J.P. Gore, R. Viskanta, Combust. Flame 111 (1997) 175–184.
[7] S. Zhdanok, L.A. Kennedy, G. Koester, Combust. Flame 100 (1995) 221–231.
[8] D.K. Min, H.D. Shin, Int. J. Heat Mass Transfer 34 (1991) 341.
[9] S.B. Sathe, R.E. Peck, T.W. Tong, Combust. Sci. Technol. 70 (4–6) (1990) 93–109.
[10] P.H. Bouma, Methane–Air Combustion on a Ceramic Foam Surface Burners, Ph.D. Dissertation, Eindhoven University of Technology, 1997.
[11] J. Buckmaster, T. Takeno, Combust. Sci. Technol. 25 (1981) 153–158.
[12] A.C. McIntosh, Dynamics of Reactive Systems: AIAA Progress in Astronautics and Aeronautic, in: Kuhl et al. (Ed.), vol. 113. AIAA, New York, 1988, pp. 385–405.
[13] A.C. McIntosh, A. Prothero, Combust. Flame 83 (1991) 111–126.
[14] R. Mital, J.P. Gore, R. Viskanta, A.C. McIntosh, Twenty-Seventh Symposium (International) on Combustion. Combustion Institute, 1988, pp. 3163–371.
[15] F.A. Lammers, L.P.H. de Goey, Combust. Flame 133 (2003) 47–61.
[16] T. Takeno, K. Sato, Combust. Sci. Technol. 20 (1–2) (1979) 73–84.
[17] Y. Katani, H.F. Behahani, T. Kakeno, Proc. Combust. Inst. (1985) 2025–2033.
[18] V.S. Babkin, A.A. Korzhavin, V.A. Bunev, Combust. Flame 87 (1991) 182–190.
[19] S.S. Minaev, S.I. Potynyakov, V.S. Babkin, Combust. Explo. Shock Waves 30 (1994) 306–310.
[20] S.G. Kim, T. Yokomori, N.I. Kim, S. Kumar, S. Maruyama, K. Maruta, Proc. Combust. Inst. 31 (2007) 2117–2124.
[21] J.G. Hoffmann, R. Echigo, H. Yoshida, S. Tada, Combust. Flame 111 (1997) 32–46.
[22] K. Hanamura, R. Echigo, Warme Stoffubertragung 26 (1991) 377–383.
[23] Y. Yoshizawa, K. Sassaki, E. Echigo, Int. J. Heat Mass Transfer 31 (2) (1988) 311–319.
[24] S.B. Sathe, R.E. Peck, T.W. Tong, Int. J. Heat Mass Transfer 33 (1990) 1331–1338.
[25] S.B. Sathe, M.R. Kulkami, R.E. Peck, T.W. Tong, Proc. Combust. Inst. 20 (1990) 1011–1018.
[26] F.M. Pereira, A. Oliveira, F. Fachini, Combust. Flame 156 (2009) 152–165.
[27] S.C. Mishra, M. Steven, S. Nemoda, P. Talukdar, D. Trims, F. Durst, Int. Commun. Heat Mass Transfer 33 (2006) 467–474.
[28] Z. Al-Hamamre, S. Diezinger, P. Talukdar, F. Von Issendorff, D. Trimis, Process Safety Environ. Prot. 84 (2006) 297–308.
[29] M. Sahraoui, M. Kaviany, Int. J. Heat Mass Transfer 37 (1994) 2817.
[30] J. Keifer, M.C. Weikl, T. Seeger, F. von Issendorff, F. Beyrau, A. Leipertz, Proc. Combust. Inst. 32 (2009) 3123–3129.
[31] M.C. Weikl, S.A. Tedder, T. Segger, Exp. Fluids 49 (2010) 775–781.
[32] M.R. Henneke, PhD Dissertation, University of Texas at Austin, 1998.
[33] M.R. Henneke, J.L. Ellzey, Combust. Flame 117 (1999) 832–840.
[34] R.J. Kee, J.F. Grcar, M.D. Smooke, J.A. Miller, Sandia National Lab., Report SAND, 1994, pp. 85–8240.
[35] R.J. Kee, G. Dixon-Lewis, J. Warnatz, M.E. Coltrin, J.A. Miller, Sandia National Lab., Report SAND, 1986, pp. 86–8246.
[36] M.D. Smooke, J. Comput. Phys. 48 (1982) 72.
[37] R.B. Brid, W.E. Stewart, E.N. Lightfoot, Transfer Phenomena, second ed., John Wiley & Sons, New York, 2002. p. 441.
[38] A.J. Barra, J.L. Ellzey, Combust. Flame 137 (2004) 230–241.